



Comparison Between Internal Steam and CO₂ Reforming of Methane for Ni-YSZ and Ni-ScSZ SOFC Anodes

Hirofumi Sumi, Yi-Hsuan Lee, Hiroki Muroyama,* Toshiaki Matsui,* and Koichi Eguchi*^z

Department of Energy and Hydrocarbon Chemistry, Graduate School of Engineering, Kyoto University, Kyoto 615-8510, Japan

The performance and durability for Ni-YSZ and Ni-ScSZ anodes of solid oxide fuel cells were compared between internal steam and CO₂ reforming of methane in the carbon deposition conditions. With a supply of H₂-CO-CO₂ mixtures to the anode, the polarization resistance increased with a rise in CO concentrations at 1023 K because of the difficulty of electrochemical oxidation of carbon monoxide. Carbon was produced by the disproportionation of carbon monoxide in CO-CO₂ mixture (CO:CO₂ = 95:5) at 1023 K, which led to low performance and much degradation of the cells. In comparison between steam and CO₂ reforming of methane, the performance and durability in a gaseous mixture at H₂O/CH₄ = 0.5 were better than that at CO₂/CH₄ = 0.5. The durability of the Ni-ScSZ anode was superior to that of the Ni-YSZ anode at 1273 K. Amorphous carbon covered the Ni-YSZ anode surface after power generation, which deactivated the nickel catalyst and inhibited gas diffusion. However, crystalline graphite with a rod morphology was grown on the Ni-ScSZ anode, which affected the catalytic activity less than amorphous carbon. The crystallinity and morphology of deposited carbon are important in determining the performance and durability of the cells at low H₂O/CH₄ and CO₂/CH₄ ratios.

© 2010 The Electrochemical Society. [DOI: 10.1149/1.3435320] All rights reserved.

Manuscript submitted February 22, 2010; revised manuscript received April 30, 2010. Published June 3, 2010.

Solid oxide fuel cells (SOFCs) are expected to be power generation systems with high energy conversion efficiency. SOFCs are generally operated at a high temperature around 1073–1273 K, which enable internal reforming of fuels such as hydrocarbon and alcohol. The internal reforming has advantages in terms of energy conversion efficiency and system simplification. However, carbon deposition must be prevented for hydrocarbon- and alcohol-fueled SOFCs. For instance, dry methane is decomposed to hydrogen and solid carbon at high temperatures. Therefore, methane fuel is generally supplied with sufficient steam for the following reaction of reforming¹



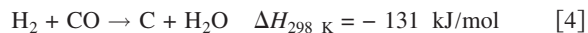
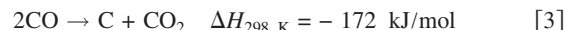
Carbon deposition can be prevented in H₂O/CH₄ ≥ 1 as far as estimated from thermodynamic equilibrium at 1273 K. At a low ratio of H₂O/CH₄ < 1, deposited carbon leads to the degradation of the anode performance due to deactivation of nickel catalyst and inhibition of fuel diffusion.² In general, the steam reforming is conducted with an excess amount of steam at approximately H₂O/CH₄ = 3. However, the high steam content also induces deterioration of the anode performance by the oxidation of nickel particles.³ A cermet composed of nickel-yttria-stabilized zirconia (Ni-YSZ) is widely used as an anode of SOFCs. Carbon deposition can be suppressed by substituting copper for nickel doping noble metals such as ruthenium.^{4,5} Continuous power generation was also reported to be possible for several hundreds of hours at a low H₂O/CH₄ ratio of 0.03, when oxygen ion conductors in the anode changed from YSZ to scandia-stabilized zirconia (ScSZ) and yttria-doped ceria.^{6,7} Especially, carbon deposited on Ni-YSZ and Ni-ScSZ anodes had different crystallinities and morphologies after power generation at H₂O/CH₄ = 0.03.⁶ Dopants to zirconia in the anode affect cell performance and durability of the cells.

Carbon dioxide reforming of methane is described by the following reaction⁸



Power generation was demonstrated with a supply of CO₂-containing gases such as biogas and anode exhaust gas.^{9,10} However, these gases include impurities, which were the main reasons of anode degradation. The compositions of biogas and exhaust gas are variable by operating conditions. Solid carbon is also depos-

ited in CO₂/CH₄ < 1 as far as estimated from thermodynamic equilibrium at 1273 K. It is important to understand the difference of anode degradation between internal steam and CO₂ reforming in the carbon deposition conditions. Furthermore, the compositions of hydrogen and carbon monoxide in reformat gases are varied with the initial H₂O/CH₄ or CO₂/CH₄ ratios and temperatures.¹¹ The H₂/CO ratios in reformat gas affect the polarization resistance of anodes at 1173–1273 K.^{2,12,13} Carbon deposition was also possible by the Boudouard reaction and reverse water gas reaction



It is important to determine which affects anode degradation, CO gas or H₂-CO mixture, in actual conditions of SOFC operations.

In this study, the performance and durability of SOFC anodes were investigated in comparison with (i) temperatures (1023–1273 K), (ii) Ni-YSZ and Ni-ScSZ anodes, (iii) CO-CO₂ and H₂-CO-CO₂ fuels, and (iv) internal steam and CO₂ reforming of methane. First, the performance and ac impedance of the anode were evaluated with a supply of simulated gases in various ratios of H₂, CO, and CO₂ at 1023–1273 K to evaluate the effect of the disproportionation and electrochemical oxidation of carbon monoxide. Second, the performance and durability were examined with a supply of methane steam or carbon dioxide mixture in H₂O/CH₄ ≤ 1 and CO₂/CH₄ ≤ 1 at 1123 and 1273 K. These conditions induce carbon deposition as far as thermodynamic equilibrium. It was reported that the performance and durability of the Ni-ScSZ anode for internal steam reforming of methane were affected by heat-treatment conditions during cell manufacturing and by the operating temperature during power generation.^{4,14–16} The internal steam and CO₂ reforming of methane were compared for the Ni-YSZ and Ni-ScSZ anodes in the carbon deposition conditions. Furthermore, the deposited carbon after power generation was analyzed by Raman spectroscopy and scanning electron microscopy (SEM). The effects of the performance and durability on the crystallinity and morphology of deposited carbon were investigated.

Experimental

Commercial YSZ [(Y₂O₃)_{0.08}-(ZrO₂)_{0.92}; Tosoh Corp.] and ScSZ [(Sc₂O₃)_{0.1}-(CeO₂)_{0.01}-(ZrO₂)_{0.89}; Daiichi Kigenso Kagaku Kogyo Co., Ltd.] were used as electrolytes. The anode cermets were prepared by mixing NiO (Wako Pure Chemical Industries, Ltd.) and YSZ (or ScSZ) powders in ethanol for 24 h; then the dried powder

* Electrochemical Society Active Member.

^z E-mail: eguchi@scl.kyoto-u.ac.jp

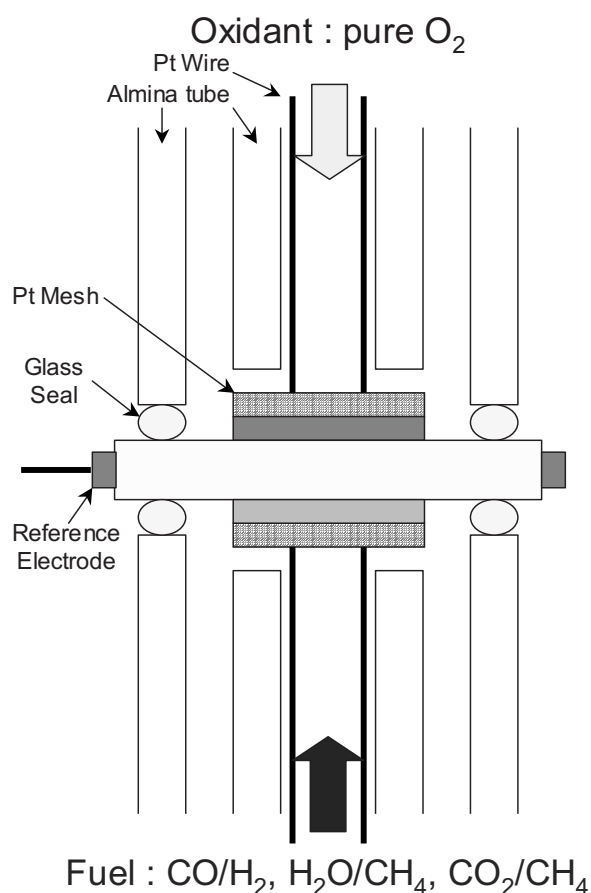


Figure 1. Schematic drawing of instrument for the evaluations of i - V characteristics and ac impedance of anode.

was fired at 1273 K for 5 h in air. The volume ratio of Ni to zirconia was 50:50 after nickel reduction. The anode layer was formed by screen printing the mixture of the cermet powders and poly(ethylene glycol) 400 on a YSZ disk (thickness: 0.5 mm and diameter: 24 mm) and by calcining at 1573 K for 5 h in air. The cathode material was perovskite oxide of $(\text{La}_{0.8}\text{Sr}_{0.2})_{0.98}\text{MnO}_{3-\delta}$ (AGC Seimi Chemical Co., Ltd.). The cathode was also formed by the screen printing procedure and by calcining at 1423 K for 5 h in air. The diameter of the electrode was 6 mm. The reference electrode of platinum wire was fixed around the YSZ disk by the use of a platinum paste.

The power generation tests were conducted at 1023, 1123, and 1273 K by using the instrument in Fig. 1. Platinum mesh and Pyrex glass were used for current collector and gas sealing, respectively. No carbon deposition was confirmed only on the platinum mesh with a supply of 100% CO or CH_4 at 1023 and 1273 K. After heating the cell to measurement temperature, 10% H_2 - N_2 mixture was supplied to the anode for nickel reduction. Then, a cell voltage of 0.7 V was kept with a supply of 5% H_2O - H_2 mixture to the anode and 100% O_2 to the cathode for 1 h until the cell performance was stabilized. A gaseous mixture of CO - CO_2 - N_2 ($\text{CO}:\text{CO}_2:\text{N}_2 = x:5:95-x$) and H_2 - CO - CO_2 - N_2 ($\text{H}_2:\text{CO}:\text{CO}_2:\text{N}_2 = 25-y:y:5:70$) was supplied to the anode. Current-voltage (i - V) characteristics were evaluated by a potentiostat/galvanostat 1470E (Solartron Analytical), and then the drawn current of 0.050 A/cm^2 was kept in $x = 95$ at 1023 K. The ac impedance of the anode was measured between the anode and reference electrode under open-circuit voltage (OCV) in the frequency range from 500 kHz to 1 Hz by an impedance analyzer 1455A (Solartron Analytical). For another series of experiment, a gaseous mixture of H_2O - or CO_2 - CH_4 - N_2 (H_2O or $\text{CO}_2:\text{CH}_4:\text{N}_2 = 5:z:95-z$) was supplied to the anode. The i - V characteristics and the ac impedance of the anodes were evalu-

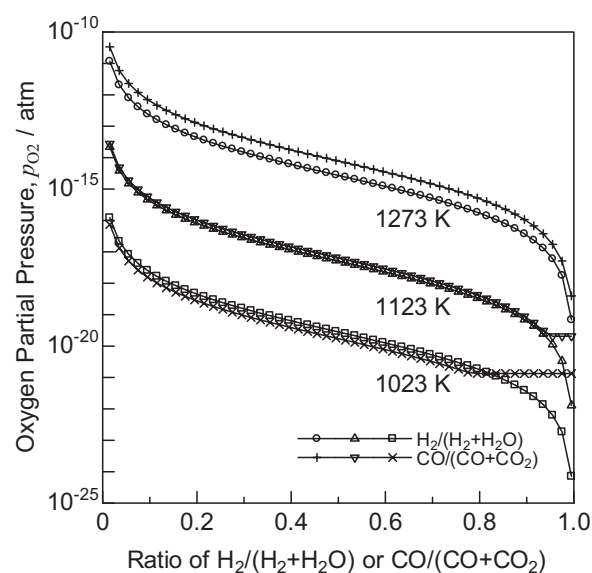


Figure 2. Calculated oxygen partial pressures as a function of $\text{H}_2/(\text{H}_2 + \text{H}_2\text{O})$ or $\text{CO}/(\text{CO} + \text{CO}_2)$ ratio at 1023, 1123, and 1273 K in equilibrium by HSC Chemistry 5.11.

ated, and then the drawn currents of 0.15 and 0.30 A/cm^2 were kept in $z = 10$ ($\text{H}_2\text{O}/\text{CH}_4 = 0.5$ or $\text{CO}_2/\text{CH}_4 = 0.5$) at 1123 and 1273 K, respectively. The total gas flow rate was 100 mL/min to the anode and cathode in every condition.

The rates of carbon deposition for Ni-YSZ and Ni-ScSZ were evaluated by thermogravimetric (TG) analysis (Shimadzu Corp. TGA-50) with a supply of dry methane at 1123 and 1273 K. The Ni-YSZ or Ni-ScSZ powder (ca. 20 mg) was put on a platinum basket in the TG system. Nitrogen was supplied with a flow rate of 90 mL/min during heating at a rate of 10 K/min, and then hydrogen was supplied with a flow rate of 30 mL/min to reduce nickel for 30 min. The weight change was measured with a supply of dry methane (20 mL/min) for 30 min at 1123 or 1273 K.

Equilibrium compositions were calculated by HSC Chemistry 5.11 (Outokumpu). The Ni-YSZ and Ni-ScSZ anodes, after power generation with a supply of $\text{H}_2\text{O}/\text{CH}_4 = 0.5$ and $\text{CO}_2/\text{CH}_4 = 0.5$, were observed by a Raman spectroscope (Horiba Jobin Yvon LabRAM HR-800) and a scanning electron microscope (Carl Zeiss NVision40). Raman spectra in 1100–1800 cm^{-1} were measured in air with the use of a 514.5 nm Ar^+ laser. The secondary electron and backscattered electron images were obtained by the scanning electron microscope with an accelerating voltage of 1 kV.

Results and Discussion

Power generation with CO - CO_2 and H_2 - CO - CO_2 mixtures.—Figure 2 shows the oxygen partial pressure calculated for the binary systems of H_2 - H_2O and CO - CO_2 at 1023, 1123, and 1273 K in equilibrium by HSC Chemistry 5.11. The oxygen partial pressure is lowered either with increasing H_2 (or CO) concentration or with decreasing temperature. The oxygen partial pressures are constant at high CO concentrations in only the CO - CO_2 system below 1123 K. In these regions, carbon is deposited by the disproportionation of carbon monoxide in equilibrium. The plateau regions expand at low temperatures. Carbon is calculated to be deposited in $\text{CO}/(\text{CO} + \text{CO}_2) \geq 0.95$ at 1123 K and in $\text{CO}/(\text{CO} + \text{CO}_2) \geq 0.79$ at 1023 K. In comparison, at the same ratios of $\text{H}_2/(\text{H}_2 + \text{H}_2\text{O})$ and $\text{CO}/(\text{CO} + \text{CO}_2)$, the oxygen partial pressure in H_2 - H_2O is larger than that in CO - CO_2 at 1023 K, whereas the opposite result is obtained at 1273 K.

Next, the performance and durability of SOFC anodes were investigated in comparison with CO - CO_2 and H_2 - CO - CO_2 fuels. Figure 3a shows the i - V characteristics with a supply of

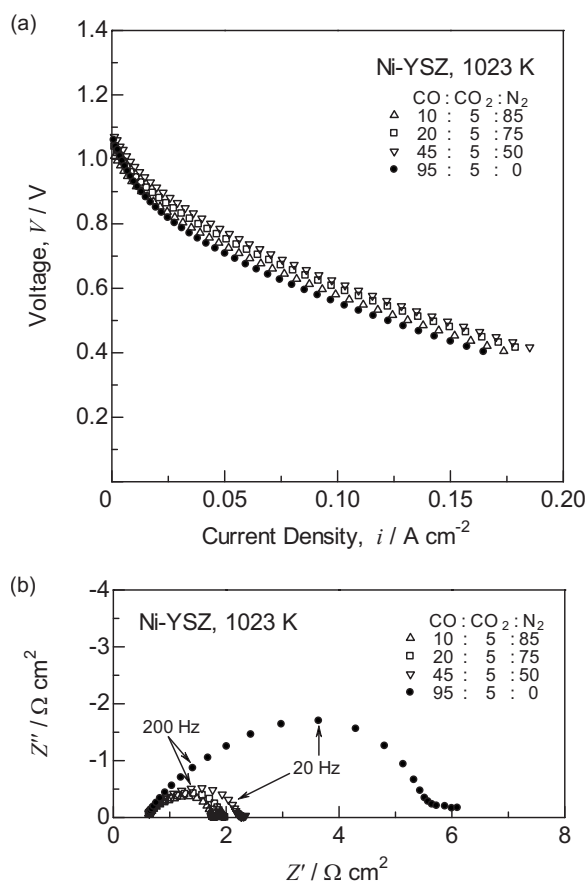


Figure 3. (a) i - V characteristics and (b) impedance spectra with a supply of CO-CO₂-N₂ mixture (CO:CO₂:N₂ = x :5:95 - x) to the Ni-YSZ anode at 1023 K.

CO-CO₂-N₂ mixture to the Ni-YSZ anode at 1023 K. An OCV rose with increasing CO concentration due to the reduction in oxygen partial pressure, as shown in Fig. 2. The OCV agreed with the theoretical electromotive force derived from the Nernst equation in the equilibrium state. The slopes of i - V curves were almost the same except for $x = 95$ in Fig. 3a. The slope for $x = 95$ was steep at low current densities. Figure 3b shows the impedance spectra of the anodes at OCVs. The arcs in the Nyquist plot became large at high CO concentrations. Especially, the arc diameter of $x = 95$ was more than 3 times as large as those of $x < 45$. Carbon is expected to be deposited at the composition of $x = 95$ in equilibrium, which leads to the large resistance such as activation and diffusion polarizations. Furthermore, the characteristic frequencies at the top of the arcs were 200 and 20 Hz at $x < 45$ and $x = 95$, respectively. Similar results were obtained in Ref. 17, which suggested the difficulty of CO electrochemical oxidation and gas diffusion due to carbon deposition.

Figure 4 shows the (a) i - V characteristics and (b) impedance spectra of the anodes with a supply of the H₂-CO-CO₂-N₂ mixture to the Ni-YSZ anode at 1023 K. The i - V curves were almost the same in every condition because of the absence of deposited carbon. However, the arcs became slightly large at high CO concentrations. The polarization resistance of $y = 25$ was larger than those in the other conditions. For the fuels containing hydrogen, steam is produced by power generation and the water gas shift reaction proceeds



However, Reaction 4 is impossible for the fuel without hydrogen because of no production of steam by power generation. The result in Fig. 4b suggests that carbon was deposited more dominantly by

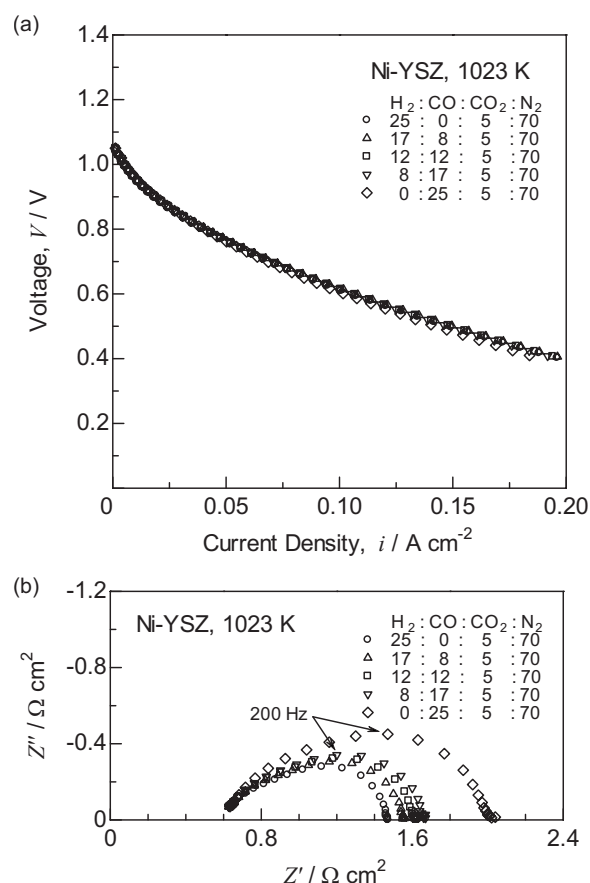


Figure 4. (a) i - V characteristics and (b) impedance spectra with a supply of H₂-CO-CO₂-N₂ mixture (H₂:CO:CO₂:N₂ = 25 - y : y :5:70) to the Ni-YSZ anode at 1023 K.

the disproportionation of carbon monoxide (Eq. 3) than by the reverse water gas reaction (Eq. 4) at 1023 K.

The same series of experiments, as shown in Fig. 3 and 4, were conducted for the Ni-YSZ and Ni-ScSZ anodes at 1123 and 1273 K. Figure 5 shows the polarization resistance of the anodes estimated from the impedance spectra as a function of CO/(H₂ + CO) and CO/(CO + CO₂) ratios at 1023, 1123, and 1273 K. The polarization

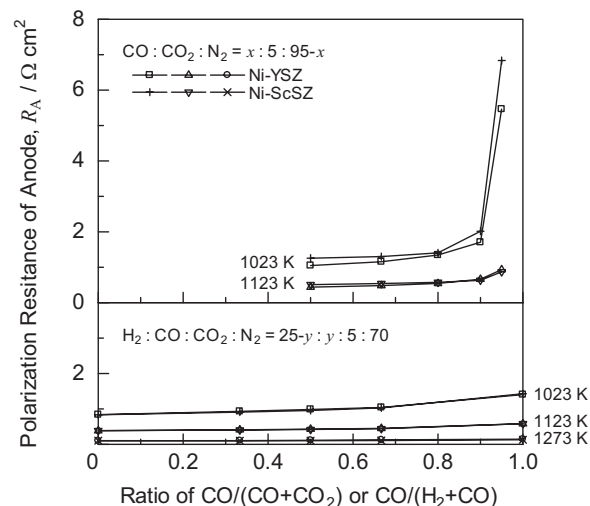


Figure 5. Polarization resistances of the Ni-YSZ and Ni-ScSZ anodes as a function of CO/(H₂ + CO) or CO/(CO + CO₂) ratio at 1023, 1123, and 1273 K.

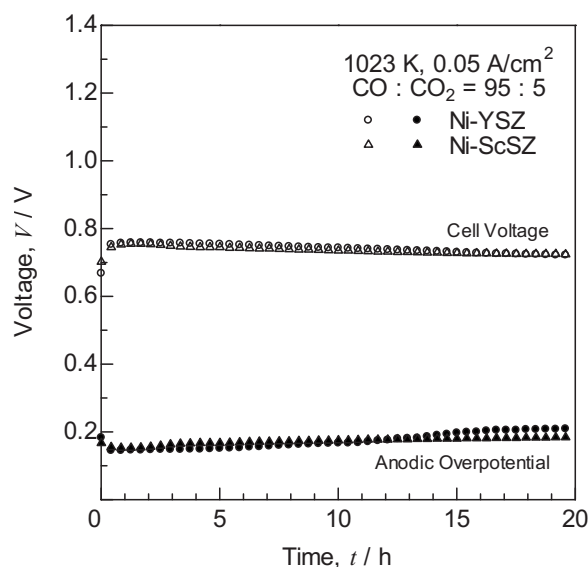
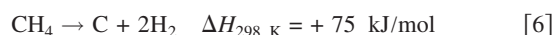


Figure 6. Time courses of cell voltage and anodic overpotential with a supply of CO–CO₂ mixture (CO:CO₂ = 95:5) to the Ni-YSZ and Ni-ScSZ anodes and a drawn current of 0.05 A/cm² at 1023 K.

resistance of the Ni-ScSZ anode was comparable to that of the Ni-YSZ anode in all conditions. The increasing rate of the polarization resistance as a function of CO concentration was large at 1023 and 1123 K. This result suggests that the electrochemical oxidation of carbon monoxide was difficult at low temperatures.

The polarization resistance increased steeply in CO/(CO + CO₂) ≥ 0.8 at 1023 K. This condition was within the carbon deposition region in Fig. 2. Figure 6 shows the time courses of cell voltage and anodic overpotential with a supply of the CO–CO₂ mixture (CO:CO₂ = 95:5) and a drawn current of 0.05 A/cm² at 1023 K. The cell voltage decreased gradually because of the increase in the anodic overpotential. The deterioration rate for the Ni-YSZ anode was almost the same (2 mV/h) as that for the Ni-ScSZ anode. After power generation, a large amount of carbon was observed on the anodes. This result supported that carbon was deposited by the disproportionation of carbon monoxide in CO/(CO + CO₂) = 0.95 at 1023 K. Power generation in the CO–CO₂ binary system becomes unstable at low temperatures.

Power generation with internal steam and CO₂ reforming of methane.— First, the region of carbon deposition was confirmed for the CO₂–CH₄ system in equilibrium. Figure 7 shows the thermodynamic equilibrium compositions in the CO₂–CH₄–N₂ mixture at 1273 K. Carbon is deposited at CO₂/CH₄ < 1 in equilibrium. This result is analogous to H₂O/CH₄ < 1 with a supply of the H₂O–CH₄–N₂ mixture.⁶ The region of carbon deposition expands at low temperatures. For instance, carbon is deposited in the region of CO₂/CH₄ < 1.5 at 1023 K. The amount of hydrogen increases with a rise in initial CH₄ composition, whereas that of carbon monoxide is unchanged. This result suggests that the cracking of methane is promoted at low CO₂/CH₄ ratios



The ratio of hydrogen and carbon monoxide depends on the initial ratio of CO₂/CH₄. For instance, the percentage of hydrogen and carbon monoxide in the gas phase at $z' = 0.10$ (CO₂/CH₄ = 0.50) are 17 and 8%, respectively, whereas those at $z' = 0.20$ (CO₂/CH₄ = 0.25) are 32 and 8%, respectively. The ratio of hydrogen and carbon monoxide is different between steam and CO₂ reforming. The percentage of hydrogen and carbon monoxide after reforming the gaseous mixture of H₂O:CH₄:N₂ = 0.05:0.10:0.85 (H₂O/CH₄ = 0.50) are 22 and 4%, respectively. The CO concentra-

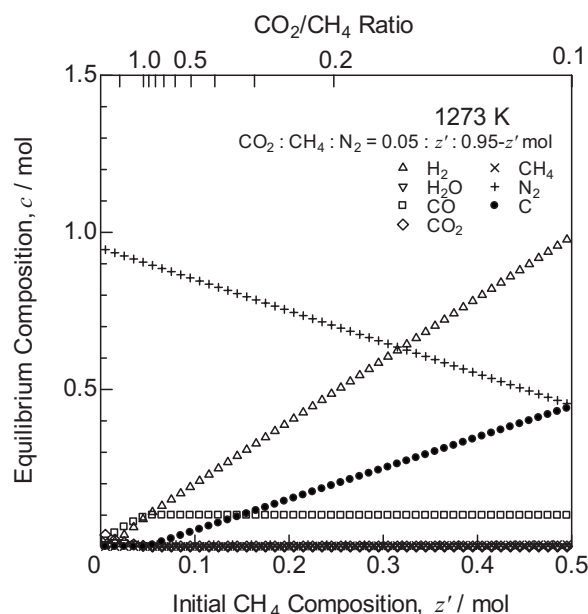


Figure 7. Thermodynamic equilibrium compositions in CO₂–CH₄–N₂ mixture (CO₂:CH₄:N₂ = 0.05:z':0.95–z') at 1273 K.

tion after CO₂ reforming is larger than that after steam reforming. The polarization resistance for CO₂ reforming is predicted to be higher due to high CO concentration than that for steam reforming.

Next, the rate of carbon deposition was evaluated with a supply of dry methane by TG analysis. Figure 8 shows the time course of weight gain by carbon deposition for the Ni-YSZ and Ni-ScSZ powders at 1123 and 1273 K. The amount of deposited carbon at 1273 K was larger than that at 1123 K because the cracking of methane was promoted at high temperatures. The rate of carbon deposition for Ni-YSZ was larger than that for Ni-ScSZ at 1273 K, whereas the order was opposite at 1123 K. Gunji et al. reported that the amount of deposited carbon was changed by heat-treatment conditions during cell manufacturing for Ni-ScSZ.¹⁴ The heat-treatment conditions affected the crystal structure of ScSZ. ScSZ with the cubic phase at

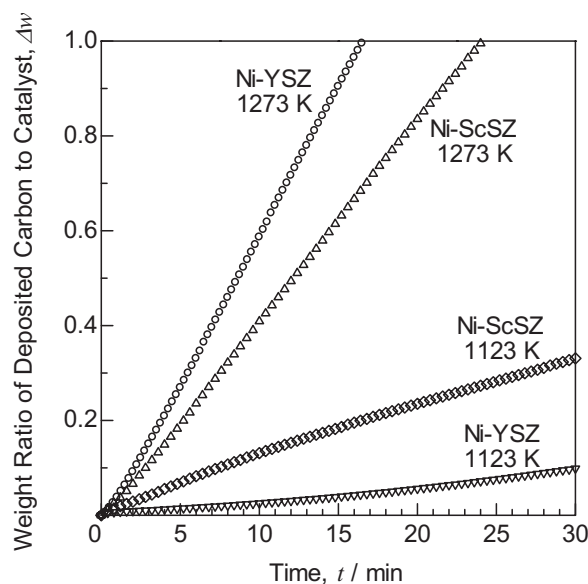
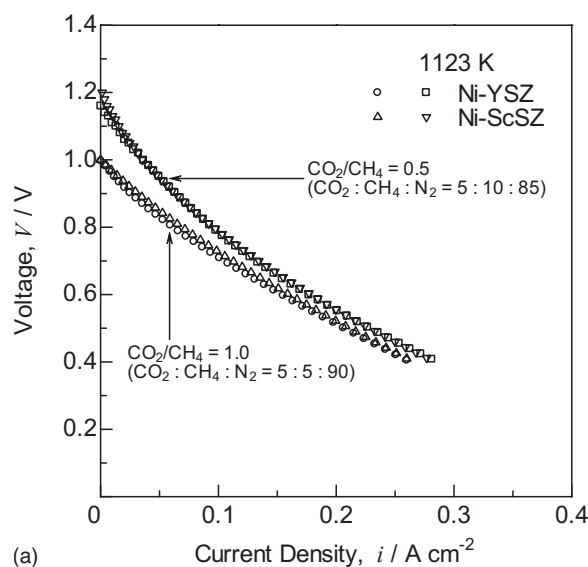
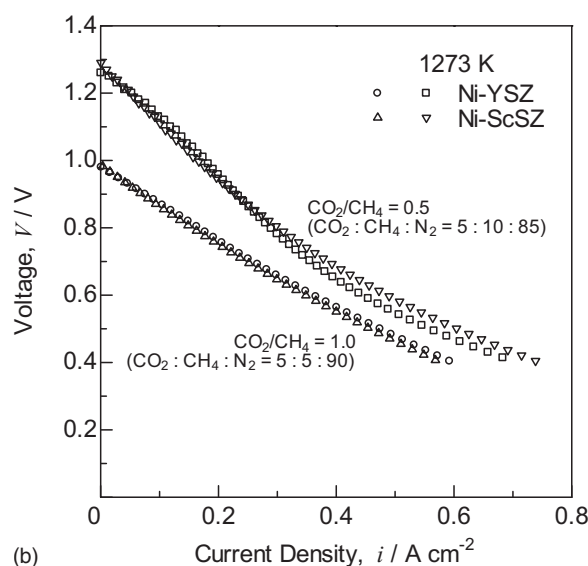


Figure 8. Time courses of weight ratio of deposited carbon to catalyst with a supply of dry methane for the Ni-YSZ and Ni-ScSZ powders at 1123 and 1273 K.



(a)



(b)

Figure 9. *i*-*V* characteristics with a supply of CO₂-CH₄-N₂ mixture (CO₂:CH₄:N₂ = 5:z:95 - z) to the Ni-YSZ and Ni-ScSZ anodes at (a) 1123 and (b) 1273 K.

room temperature facilitated carbon deposition as compared with the rhombohedral phase. Furthermore, an additive of Al₂O₃, Bi₂O₃, Ga₂O₃, or CeO₂ in ScSZ led to the stabilization of the cubic phase at room temperature.¹⁸⁻²⁰ In this study, 1 mol % of CeO₂-doped ScSZ was used. The crystalline structure was confirmed to be cubic for both YSZ and ScSZ at every temperature by X-ray diffraction. The results in Fig. 8 suggest that the rate of carbon deposition was affected by the dopant in zirconia and by the operating temperature.

Figure 9 shows the *i*-*V* characteristics with a supply of CO₂/CH₄ = 0.5 and 1.0 to the Ni-YSZ and Ni-ScSZ anodes at (a) 1123 and (b) 1273 K. At CO₂/CH₄ = 0.5, the OCV was ~1.2 and 1.3 V at 1123 and 1273 K, respectively, which almost agreed with the theoretical value derived from the equilibrium compositions in Fig. 7. The slope of the *i*-*V* curve at CO₂/CH₄ = 0.5 in the carbon deposition condition was steeper than that at CO₂/CH₄ = 1.0 in a region of low current densities at 1123 and 1273 K. However, the slopes at CO₂/CH₄ = 0.5 and 1.0 were almost the same at high current densities. Steam and carbon dioxide were produced by the power generation at high current densities, which promoted reforming of methane, as expressed by Reactions 1 and 2. The cell perfor-

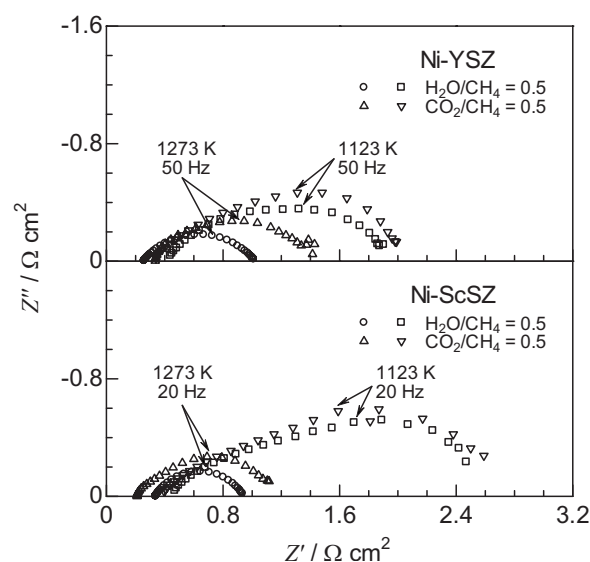


Figure 10. Impedance spectra with a supply of H₂O or CO₂-CH₄-N₂ mixture (H₂O or CO₂:CH₄:N₂ = 5:10:85) to the Ni-YSZ and Ni-ScSZ anodes at 1273 K.

mance for the Ni-YSZ anode was lower than that for the Ni-ScSZ anode at CO₂/CH₄ = 0.5 in the carbon deposition condition at 1273 K. The impedance spectra of the anodes at OCV were obtained as shown in Fig. 10. The polarization resistance of the Ni-YSZ anode was larger than that of the Ni-ScSZ anode at 1273 K because carbon was deposited more easily as was observed by TG analysis, as shown in Fig. 8. On the contrary, the resistance of the Ni-YSZ anode was smaller than that of the Ni-ScSZ anode at 1123 K. This result also corresponds to the TG analysis. Thus, the rate of carbon deposition was closely related to the polarization resistance of the Ni-YSZ and Ni-ScSZ anodes. In comparison between steam and CO₂ reforming, the polarization resistance in H₂O/CH₄ = 0.5 was smaller than that in CO₂/CH₄ = 0.5 for both of the Ni-YSZ and Ni-ScSZ anodes at 1273 K. This result suggested that the reforming of methane and electrochemical oxidation of fuel for steam reforming were promoted more than that for CO₂ reforming in the carbon deposition condition.

Short-term durability was evaluated for Ni-YSZ and Ni-ScSZ anodes in the carbon deposition conditions. Figure 11 shows the time courses of cell voltage and anodic overpotential in H₂O/CH₄ = 0.5 and CO₂/CH₄ = 0.5 at 1123 and 1273 K. At 1123 K, no degradation was observed for the Ni-YSZ anode, whereas the cell voltage decreased slightly for the Ni-ScSZ anode. The decreasing rate of cell voltage corresponded to the increasing rate of anodic overpotential. The polarization resistances of the anodes were also reported to increase with elapsed time, which was mainly caused by carbon deposition.²¹ At 1273 K, the degradation rate for the Ni-YSZ anode was larger than that for the Ni-ScSZ anode. Shiratori and Sasaki also reported the stable power generation with a supply of CO₂-CH₄ mixture for the Ni-ScSZ anode.²² The cell voltage and anodic overpotential were stable during steam reforming for the Ni-ScSZ anode. Furthermore, both of the Ni-YSZ and Ni-ScSZ anodes were promoted to deteriorate for CO₂ reforming at 1273 K. Table I summarizes the initial polarization resistances of the Ni-YSZ and Ni-ScSZ anodes and the increasing rates of anodic overpotential for the initial 20 h with supplies of H₂O/CH₄ = 0.5 and CO₂/CH₄ = 0.5 at 1123 and 1273 K. The initial polarization resistance of the anodes for CO₂ reforming was larger than that for steam reforming. The resistance was larger for the Ni-ScSZ anode at 1123 K and for Ni-YSZ anode at 1273 K. In the durability test, the change in anodic overpotential was less than 1 mV/h for the initial 20 h at 1123 K. However, the degradation of the Ni-YSZ anode was remarkable at 1273 K. The

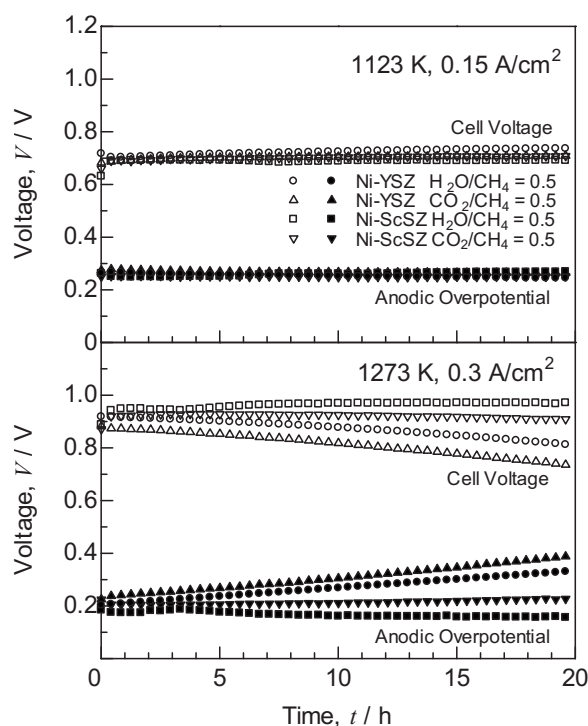


Figure 11. Time courses of cell voltage and anodic overpotential with a supply of H₂O or CO₂-CH₄-N₂ mixture (H₂O or CO₂:CH₄:N₂ = 5:10:85) to the Ni-YSZ and Ni-ScSZ anodes at 1123 and 1273 K.

increasing rate of anodic overpotential was 8.6 mV/h for CO₂ reforming, which is larger than that for steam reforming at 1273 K.

After power generation, the deposited carbon on the Ni-YSZ and Ni-ScSZ anodes was observed by Raman spectroscopy and SEM. Figure 12 shows the Raman spectra after power generation in H₂O/CH₄ = 0.5 and CO₂/CH₄ = 0.5 at 1123 and 1273 K. Two peaks at ~1350 cm⁻¹ (D-band) and 1580 cm⁻¹ (G-band) were attributable to amorphous carbon and crystalline graphite, respectively. At 1123 K, small peaks of the G-band were observed in every condition. This result supported that the suppression of carbon deposition enabled the low degradation rate, as shown in Fig. 11. Yamaji et al. observed the strong G-band after exposure to 1.2% H₂O-CH₄ without current loading at 1073 K.²³ Pomfret et al. reported that the intensity of the G-band decreased with a rise in current density because of the electrochemical oxidation of deposited carbon.²⁴ The G-band became small because of the current loading of 0.15 A/cm² at 1123 K in this study. The intensity of the G-band gained at a high temperature of 1273 K. Furthermore, the intensity of the D-band increased only for the Ni-YSZ anode. The ratios of peak intensities between the D-band and G-band (I_D/I_G) were 0.25 and 0.75 for the

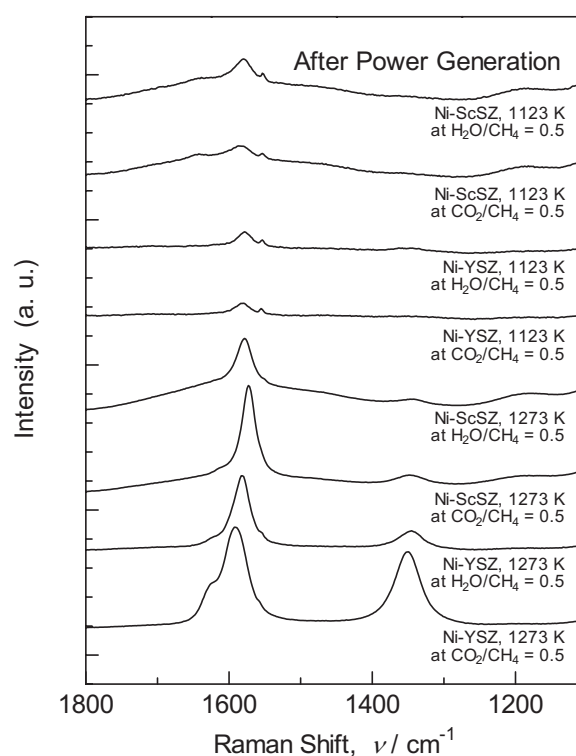


Figure 12. Raman spectra for the Ni-YSZ and Ni-ScSZ anodes after power generation with a supply of H₂O or CO₂-CH₄-N₂ mixture (H₂O or CO₂:CH₄:N₂ = 5:10:85) at 1123 and 1273 K.

Ni-YSZ anode after power generation in H₂O/CH₄ = 0.5 and CO₂/CH₄ = 0.5, respectively. The degradation rate was the largest for the Ni-YSZ anode in CO₂/CH₄ = 0.5, as shown in Fig. 11. Therefore, it is likely that the deposition of amorphous carbon gave rise to the deterioration of the cell performance.

Figure 13 shows the SEM images for the Ni-YSZ and Ni-ScSZ anodes after power generation in H₂O/CH₄ = 0.5 and CO₂/CH₄ = 0.5 at 1273 K. The black areas in the backscattered electron images were ascribed to deposited carbon by an energy-dispersive X-ray spectrometer with an accelerating voltage of 10 kV. Two morphological types of deposited carbon were observed on the Ni-YSZ anode. One was a gumlike carbon marked with dotted lines, and the other was carbon with an angular surface covering on Ni particles marked with solid lines. The gumlike carbon was observed only on the Ni-YSZ anode, which corresponded to amorphous carbon judging from the Raman spectra in Fig. 12. This carbon was likely to cause deterioration by not only the decrease in catalytic activity but also the inhibition of gas diffusion. The amorphous carbon was more abundantly observed after CO₂ reforming than after steam reform-

Table I. Initial polarization resistances of the Ni-YSZ and Ni-ScSZ anodes and increasing rates of anodic overpotential for initial 20 h with supplies of H₂O/CH₄ = 0.5 and CO₂/CH₄ = 0.5 at 1123 and 1273 K.

Temperature (K)	Anode	Fuel	Initial polarization resistance of anode (Ω cm ²)	Increasing rate of anodic overpotential (mV/h)
1123	Ni-YSZ	H ₂ O/CH ₄ = 0.5	1.5	-0.9
		CO ₂ /CH ₄ = 0.5	1.7	-0.5
	Ni-ScSZ	H ₂ O/CH ₄ = 0.5	2.0	0.3
		CO ₂ /CH ₄ = 0.5	2.2	0.1
1273	Ni-YSZ	H ₂ O/CH ₄ = 0.5	0.75	6.5
		CO ₂ /CH ₄ = 0.5	1.1	8.3
	Ni-ScSZ	H ₂ O/CH ₄ = 0.5	0.60	-1.2
		CO ₂ /CH ₄ = 0.5	0.91	0.3

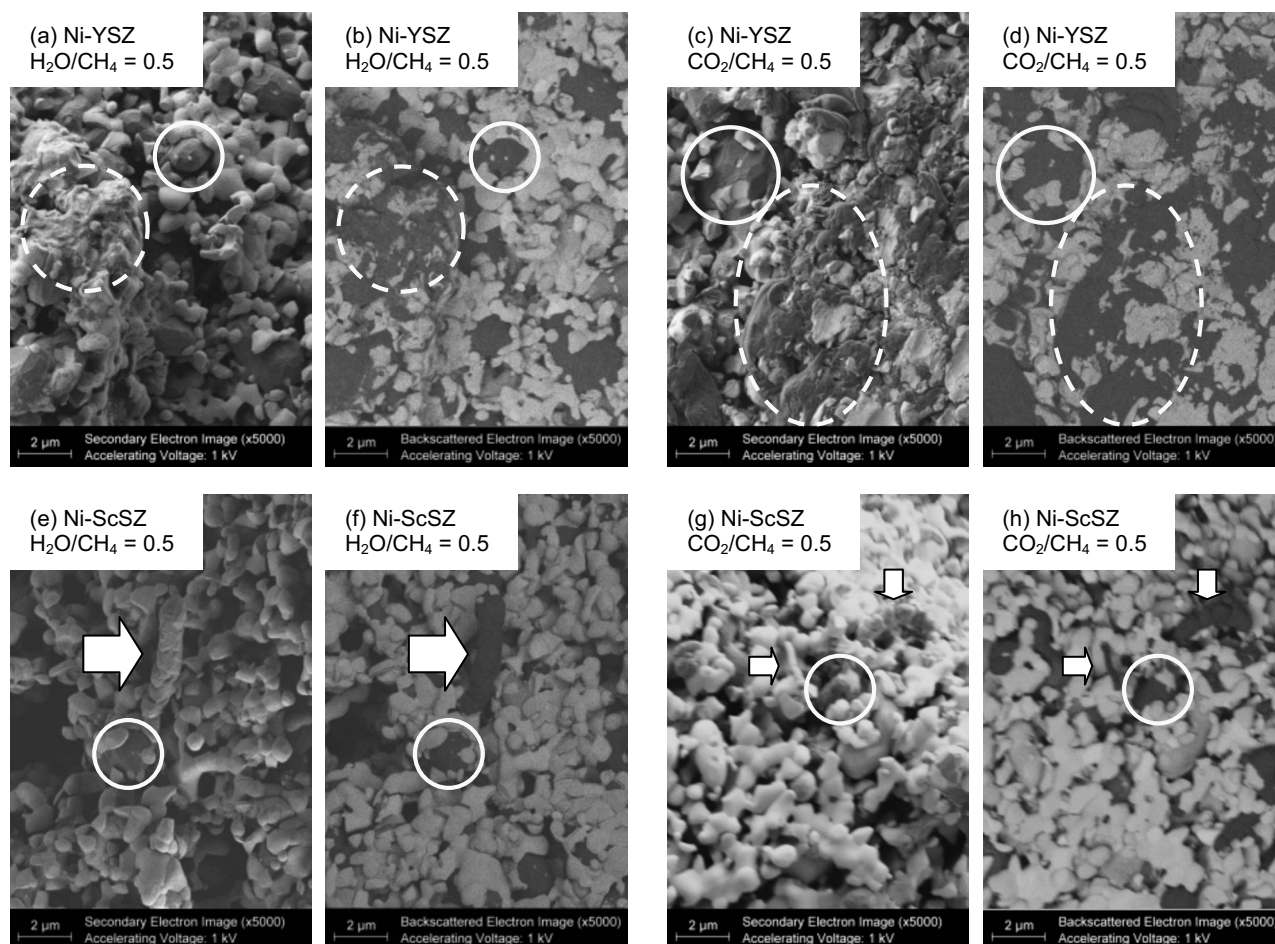


Figure 13. SEM images for the [(a)-(d)] Ni-YSZ and [(e)-(h)] Ni-ScSZ anodes after power generation. a, b, e, and f are at $\text{H}_2\text{O}/\text{CH}_4 = 0.5$ and c, d, g, and h are at $\text{CO}_2/\text{CH}_4 = 0.5$ at 1273 K. a, c, e, and g are secondary electron images, and b, d, f, and h are backscattered electron images.

ing. The angular carbon was also observed on the Ni-ScSZ anode, which corresponded to graphite. This carbon was expected to be electrically conductive as compared to the amorphous one, although it caused the deactivation of the nickel catalyst. Furthermore, the rod-shaped carbon was observed only on the Ni-ScSZ anode marked with arrows in Fig. 13. The rod-shaped carbon with various radii was confirmed after CO_2 reforming. This carbon, being ascribed to crystalline graphite due to the absence of the D-band, did not cover Ni particles. This rod-shaped graphite affected the catalytic activity less than the amorphous carbon. The crystallinity and morphology of deposited carbon strongly influenced the performance and durability at low $\text{H}_2\text{O}/\text{CH}_4$ and CO_2/CH_4 ratios.

Conclusion

In this study, the cell performance and ac impedance of the Ni-YSZ and Ni-ScSZ anodes were evaluated in simulated gases with various ratios of H_2 , CO , and CO_2 . The polarization resistance increased with a rise in CO concentration at low temperatures because of the difficulty of electrochemical oxidation of carbon monoxide. Carbon was deposited by the disproportionation of carbon monoxide in the $\text{CO}-\text{CO}_2$ mixture ($\text{CO}:\text{CO}_2 = 95:5$) at 1023 K, which led to degraded performance. The durability for the Ni-YSZ and Ni-ScSZ anodes was also examined in comparison with internal steam and CO_2 reforming of methane. The amount of deposited carbon at 1273 K was larger than that at 1123 K because the cracking of methane was facilitated at high temperatures. The descending order of degradation rate was Ni-YSZ (CO_2) > Ni-YSZ (steam) > Ni-ScSZ (CO_2) > Ni-ScSZ (steam) at 1273 K. Amorphous car-

bon was observed only on the Ni-YSZ anode, which was likely to cause deterioration by the decrease in nickel catalytic activity and the inhibition of gas diffusion. In contrast, the crystalline rod-shaped graphite was observed only on the Ni-ScSZ anode. The cell voltage and anodic overpotential were stable for the Ni-ScSZ anode. The crystallinity and morphology of deposited carbon strongly influenced the performance and durability of the cells at low $\text{H}_2\text{O}/\text{CH}_4$ and CO_2/CH_4 ratios.

Kyoto University assisted in meeting the publication costs of this article.

References

1. K. Eguchi, H. Kojo, T. Takeguchi, R. Kikuchi, and K. Sasaki, *Solid State Ionics*, **152-153**, 411 (2002).
2. T. Takeguchi, Y. Kani, T. Yano, R. Kikuchi, K. Eguchi, K. Tsujimoto, Y. Uchida, A. Ueno, K. Omoshiki, and M. Aizawa, *J. Power Sources*, **112**, 588 (2002).
3. T. Matsui, R. Kishida, J.-Y. Kim, H. Muroyama, and K. Eguchi, *J. Electrochem. Soc.*, **157**, B776 (2010).
4. S. Park, R. J. Gorte, and J. M. Vohs, *J. Electrochem. Soc.*, **146**, 3603 (1999).
5. T. Takeguchi, R. Kikuchi, T. Yano, K. Eguchi, and K. Murata, *Catal. Today*, **84**, 217 (2003).
6. H. Sumi, K. Ukai, Y. Mizutani, H. Mori, C.-J. Wen, H. Takahashi, and O. Yamamoto, *Solid State Ionics*, **174**, 151 (2004).
7. E. P. Murray, T. Tsai, and S. A. Barnett, *Nature (London)*, **400**, 19 (1999).
8. Z. Gao, K. Sekizawa, and K. Eguchi, *Electrochemistry (Tokyo, Jpn.)*, **67**, 336 (1999).
9. Y. Shiratori, T. Oshima, and K. Sasaki, *Int. J. Hydrogen Energy*, **33**, 6316 (2008).
10. R. Peters, E. Riensche, and P. Cremer, *J. Power Sources*, **86**, 432 (2000).
11. K. Sasaki and Y. Teraoka, *J. Electrochem. Soc.*, **150**, A878 (2003).
12. K. Sasaki, Y. Hori, R. Kikuchi, K. Eguchi, A. Ueno, H. Takeuchi, M. Aizawa, K. Tsujimoto, H. Tajiri, H. Nishikawa, et al., *J. Electrochem. Soc.*, **149**, A227 (2002).
13. A. Weber, B. Sauer, A. C. Müller, D. Herbstritt, and E. Ivers-Tiffée, *Solid State Ionics*, **152-153**, 543 (2002).

14. A. Gunji, C. Wen, J. Otomo, T. Kobayashi, K. Ukai, Y. Mizutani, and H. Takahashi, *J. Power Sources*, **131**, 285 (2004).
15. K. Ke, A. Gunji, H. Mori, S. Tsuchida, H. Takahashi, K. Ukai, Y. Mizutani, H. Sumi, M. Yokoyama, and K. Waki, *Solid State Ionics*, **177**, 541 (2006).
16. T. Matsui, T. Iida, R. Kikuchi, M. Kawano, T. Inagaki, and K. Eguchi, *J. Electrochem. Soc.*, **155**, B1136 (2008).
17. V. Alzate-Restrepo and J. M. Hill, *J. Power Sources*, **195**, 1344 (2010).
18. M. Mizutani, M. Tamura, M. Kawai, and O. Yamamoto, *Solid State Ionics*, **72**, 271 (1994).
19. Y. Arachi, T. Asai, O. Yamamoto, Y. Takeda, N. Imanishi, K. Kawate, and C. Tamakoshi, *J. Electrochem. Soc.*, **148**, A520 (2001).
20. M. Hirano, T. Oda, K. Ukai, and Y. Mizutani, *Solid State Ionics*, **158**, 215 (2003).
21. J.-H. Koh, Y.-S. Yoo, J.-W. Park, and H. C. Lim, *Solid State Ionics*, **149**, 157 (2002).
22. Y. Shiratori and K. Sasaki, *J. Power Sources*, **180**, 738 (2008).
23. K. Yamaji, H. Kishimoto, Y. Xiong, T. Horita, N. Sakai, M. E. Brito, and H. Yokokawa, *Solid State Ionics*, **179**, 1526 (2008).
24. M. B. Pomfret, J. Marda, G. S. Jackson, B. W. Eichhorn, A. M. Dean, and R. A. Walker, *J. Phys. Chem. C*, **112**, 5232 (2008).